ISSN 0036-0236, Russian Journal of Inorganic Chemistry, 2014, Vol. 59, No. 11, pp. 1219–1227. © Pleiades Publishing, Ltd., 2014.
Original Russian Text © P.V. Evdokimov, V.I. Putlyaev, V.K. Ivanov, A.P. Garshev, T.B. Shatalova, N.K. Orlov, E.S. Klimashina, T.V. Safronova, 2014, published in Zhurnal Neorganicheskoi Khimii, 2014, Vol. 59, No. 11, pp. 1462–1471.

SYNTHESIS AND PROPERTIES OF INORGANIC COMPOUNDS

Phase Equilibria in the Tricalcium Phosphate–Mixed Calcium Sodium (Potassium) Phosphate Systems

P. V. Evdokimov[a], V. I. Putlyaev[a], V. K. Ivanov[a, b], A. P. Garshev[a], T. B. Shatalova[a], N. K. Orlov[a], E. S. Klimashina[a], and T. V. Safronova[a]

[a] *Lomonosov Moscow State University, Leninskie Gory, Moscow 119991, Russia*
[b] *Kurnakov Institute of General and Inorganic Chemistry, Russian Academy of Sciences, Leninskii pr. 31, Moscow 119991, Russia*
e-mail: pavel.evdokimov@gmail.com

Received May 23, 2013

Abstract—Phase equilibria in the quasi-binary sections $Ca_3(PO_4)_2$–$CaMPO_4$ (M = Na, K) are distinguished by high-temperature isomorphism of glaserite-like phases α'-$Ca_3(PO_4)_2$ and α-$CaMPO_4$. The main differences of the $Ca_3(PO_4)_2$–$CaKPO_4$ system from the $Ca_3(PO_4)_2$–$CaNaPO_4$ system are a shift of invariant equilibria toward higher temperatures, deceleration of phase transformations, and the emergence of polymorphism of an intermediate phase of an ordered solid solution based on α-$CaKPO_4$. The low-temperature modification of this phase of a composition near $Ca_8K_2(PO_4)_6$ has the apatite structure with unoccupied hexagonal channels.

DOI: 10.1134/S0036023614110084

An important area of modern inorganic materials science is the development of biomaterials based on calcium phosphate for replacing or healing damaged bone tissue. Ideally, an implant should gradually dissolve in the medium of the body while performing support functions and be replaced by new bone tissue. In this context, the key characteristic of a material is its ability to be resorbed by, i.e., to dissolve in the medium of the body. Traditionally used hydroxyapatite $Ca_{10}(PO_4)_6(OH)_2$ is the lowest soluble calcium phosphate [1].

A necessary element of a strategy of improving the solubility of a compound with ionic chemical bonds is to decrease the crystal lattice energy. Consistent implementation of this approach leads to two methods for increasing the resorbability of calcium phosphate materials. The first method is to switch to calcium phosphates for which the Ca : P ratio is lower than that in hydroxyapatite (for example, a switch from hydroxyapatite with a Ca : P ratio of 1.67 to tricalcium phosphate (TCP) β-$Ca_3(PO_4)_2$ with a Ca : P ratio of 1.5 leads to an increase in the solubility by an order of magnitude). The second method is to modify the chemical composition by replacing the cation Ca^{2+} in the phosphate (e.g., TCP) structure by a singly charged alkali metal cation; the replacement causes a change in the structural type β-TCP → β-$CaMPO_4$ (rhenanite). This work focuses on using mixed calcium alkali metal phosphates with the general formula $Ca_{3-x}M_{2x}(PO_4)_2$ (x = 0–1, M = Na, K) with the structures of TCP and $CaMPO_4$ as resorbable bioceramics.

A similar challenge—conversion of slightly soluble phosphorites to phosphate forms assimilable by plants—occurred previously in phosphate fertilizer technology. A possible solution is heat treatment of phosphorites in the Rhenania process—calcination of phosphorites with alkali metal carbonates and silica. One of the products of such a process is rhenanite $CaMPO_4$. The main experimental efforts to analyze the phase equilibria and the crystal chemistry of phases in the systems M_2O–CaO–P_2O_5 (M = K, Na) [2–5], among which Bredig's fundamental work [6], were made in the 1950–1980s. An analysis of these experimental results showed that it is required to reconsider phase relationships in the quasi-binary section $Ca_3(PO_4)_2$–$CaNaPO_4$ and to construct the phase diagram of the $Ca_3(PO_4)_2$–$CaKPO_4$ system (on this diagram, we failed to find any data). In addition, in the context of using mixed calcium alkali metal phosphates as bioceramics, it is necessary to have a clear idea of structural features of phases constituting these systems and their polymorphism. Unfortunately, such data, particularly those on the K-containing system, are fragmentary and quite contradictory. The above aspects of the chemistry of mixed calcium alkali metal phosphates are the subject of this work.

EXPERIMENTAL

For the synthesis, the following reactions of synthesis of binary phosphates were chosen:

$$Ca_2P_2O_7 + (1-x)CaCO_3 + xM_2CO_3 \rightarrow Ca_{3-x}M_{2x}(PO_4)_2 + CO_2\uparrow, \quad (1)$$

$$Ca_2P_2O_7 + (1-x)CaCO_3 + 2xMCl + H_2O \rightarrow Ca_{3-x}M_{2x}(PO_4)_2 + 2HCl\uparrow + CO_2\uparrow, \quad (2)$$

where M = Na, K and $x = 0$–1.

The initial reaction mixture was ground in a Pulverisette planetary ball mill (Fritsch, Germany) in an acetone medium. The ground reaction mixture was rubbed through a Saatilene HiTech™ polyester mesh (~200 μm), placed in an alundum crucible, and calcined within the temperature range 800–1100°C for up to 12 h. For subsequent compaction of ceramic pellets, into the disaggregated calcined powders, a plasticizer (paraffin, 10% of powder weight) was introduced. From the press powder, pellets were compacted by uniaxial single-action pressing in a Carver C hand press (USA) at a pressure of ~200 MPa and then sintered at 1200°C.

High-temperature X-ray powder diffraction experiments were carried out in situ within the temperature range 50–1350°C using an HT 1500 high temperature attachment with a Rigaku D/MAX 2500 rotating-anode diffractometer (Rigaku, Japan) in the Bragg–Brentano geometry using CuK_α radiation ($\lambda = 1.54183$ Å) at an accelerating voltage of 40 kV and a tube current of 200 mA in a platinum cell. Profile analysis of spectra and determination of unit cell parameters were performed with the WinXPOW software (STOE GmbH).

The quantitative composition of the mixture was determined both using a calibration function and nonoverlapping analytical diffraction peaks, and using the corundum number I/I_c by the Chung method [7]. At known values of the corundum number, we have $\Sigma\omega_k = 1$, where $k = 1, 2, 3, \ldots$, where ω_k are the mass fractions of components. The mass fraction is calculated as

$$\omega_A = \frac{I_{iA}\Big/(I/I_c(A)I_{iA}^{rel})}{\sum\limits_k I_{iK}\Big/(I/I_c(K)I_{iK}^{rel})}, \quad (3)$$

where I_{iA} is the measured intensity of the ith reflection of the phase A; I_{iA}^{rel} is the relative intensity of this reflection in a database; $I/I_c(A)$ is the corundum number of the phase A; and I_{iK}, I_{iK}^{rel}, and $I/I_c(K)$ are the respective quantities for all the components (including A) of the mixture.

Differential thermal and thermogravimetric analyses of samples were performed with an STA 409 PC Luxx top-loading simultaneous thermal analyzer (Netzsch, Germany). The measurements were made in an air atmosphere in alundum crucibles within the temperature range from room temperature to 1480°C at a heating rate of 5–50 deg/min. The sample weights were up to 130 mg.

The linear shrinkage of the pressed samples was measured in polythermal mode to 1400°C at a heating rate of 5 deg/min in a DIL 402 C horizontal dilatometer (Netzsch, Germany).

RESULTS AND DISCUSSION

Selection of Conditions for Synthesizing Powder Samples

The thermolysis of alkali metal chloride and the release of hydrogen chloride (reaction (2)) were confirmed by thermogravimetric experiments with IR analysis of the released gases (a characteristic peak of vibrations of HCl molecule at 3000 cm^{-1}). The thermodynamics of reactions (1) and (2) is determined by both the enthalpy contribution (the formation of mixed orthophosphate, a compound the crystal lattice energy of which is higher than that of calcium pyrophosphate because orthophosphate is a more compact anion), and the entropy contribution (an increase in the number of moles of gaseous products in these reactions).

Processing the data of the thermogravimetry at various heating rates using two different models (by Ozawa, Flynn, and Wall [8, 9] and by Vyazovkin [10]) estimated the activation energy of rhenanite formation reaction (1) (or, more precisely, its low-temperature (<660°C) stage) at 90 ± 10 kJ/mol. Such a low value of the activation energy is likely to suggest that, in terms of limiting process, the control of this reaction is intermediate between the kinetic control (interface reaction) and the control by diffusion. The temperatures at which reactions (1) and (2) begin (~600°C for carbonate and ~750°C for chloride) are within the temperature range preceding the melting point of the corresponding sodium precursor; i.e., the initial stages of reactions (1) and (2) are most probably solid-phase reactions. The change in the homogeneity of the powder (by grinding in the planetary ball mill for higher dispersity and better mixing) shifts the completion of the reaction toward lower temperatures. In particular, using the planetary ball mill for grinding the mixture of reactants reduced the average particle size in the initial mixtures to 7 μm. Because of this, the temperatures of the completion of the reactions significantly decrease (to 680 and 790°C for Na_2CO_3 and NaCl, respectively).

Note that rhenanite (the composition at $x = 1$) begins to form at lower temperature than tricalcium phosphate (the composition at $x = 0$). Because the rearrangement of the calcium pyrophosphate crystal lattice in the reactions $Ca_2P_2O_7 + Na_2CO_3 = 2CaNaPO_4 + CO_2$ and $Ca_2P_2O_7 + CaCO_3 = Ca_3(PO_4)_2$ is quite significant and requires the P–O bond in the pyrophosphate ion to break down and then the forming orthophosphate ions to move apart, the difference in temperatures of the onset and comple-

tion if the reactions is likely to be due to the difference in diffusion mobility between the Na^+ and Ca^{2+} ions. In its turn, this allows one to represent each of the reactions as the diffusion of Na^+, Ca^{2+}, and O^{2-} ions into a calcium pyrophosphate particle through a product layer.

The isothermal experiments demonstrated that the β-$CaNaPO_4$ synthesis temperature can be reduced to 600°C (the reaction was performed for 4 h). At this temperature, there is a weight loss, which agrees with that calculated theoretically. This is owing to the complete removal of carbon dioxide in the decomposition of sodium carbonate, which cannot decompose at this temperature by any reaction other than reaction (1). Thus, slow heating of the reaction mixtures enables one to carry out the process in the presence of a minimal amount of the melt (and, probably, even in solid-phase mode). Annealing at 900°C for 4 h guarantees the production of single-phase TCP or rhenanite even without repeated grinding and calcination of the reaction mixture.

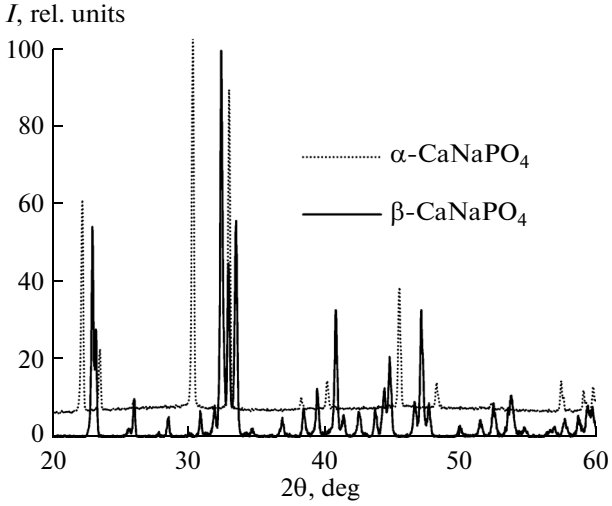

Fig. 1. Comparison of the X-ray powder diffraction data on the low-temperature modification β-$CaNaPO_4$ and the high-temperature modification α-$CaNaPO_4$.

$Ca_3(PO_4)_2$ Polymorphism

In the references cited in this work, there are disagreements about the number of polymorphic modifications of the TCP phase. According to our data [11], the transition β → α-TCP is a first-kind hindered reconstructive transition with ΔH = 6.8 kJ/mol and $\Delta V/V$ = +4.5%; the transformation begins at 1183°C and requires calcination at 1400°C for ~1 h for completion. In the reverse transition, the supercooling can exceed 300°C. This makes it possible to produce the high-temperature phase α-$Ca_3(PO_4)_2$ even while not too rapid cooling (about 5 deg/min). The transition α → α'-TCP is a first-kind fast deformation transition with ΔH = 10.73 kJ/mol; the transition begins at 1455°C and has low temperature hysteresis Δt = 20°C. This eliminates the possibility of obtaining α'-$Ca_3(PO_4)_2$ even while quenching.

$CaNaPO_4$ Polymorphism

For $CaNaPO_4$, two modifications are known [5]: the high-temperature α-$CaNaPO_4$ and the low-temperature β-$CaNaPO_4$ with the transition temperature T = 690°C. Figure 1 presents the X-ray powder diffraction data on the phases α-$CaNaPO_4$ and β-$CaNaPO_4$.

The X-ray powder diffraction data on α-$CaNaPO_4$ were compared with the known ICDD PDF-2 card No. 74-1950 for this phase, which was obtained by Bredig [6]. Our X-ray powder diffraction data show more reflections than Bredig's, and these reflections are fully indexable within the hexagonal symmetry (assumed symmetry group $P\bar{3}m1$) with the unit cell parameters a = 5.23 Å and c = 7.24 Å.

The differential thermal analysis study of the polymorphic transformation was performed according to a published procedure [11]. According to the data of the study (Fig. 2), the temperature of the transition β → α-$CaNaPO_4$ is 670°C. This transition is accompanied by an abrupt endothermic event while heating, which is virtually equal in energy ($\Delta H_{\beta/\alpha} = 8.22 \pm 0.16$ kJ/mol) to the exothermic event accompanying the transition α → β-$CaNaPO_4$ while cooling ($\Delta H_{\alpha/\beta} = 8.06 \pm 0.16$ kJ/mol); the temperature hysteresis is ΔT = 10°C. The dilatometric study demonstrated that the transition β → α-$CaNaPO_4$ is accompanied by a positive volume change $\Delta V/V$ = +6%; the high-temperature X-ray powder diffraction analysis gave a similar estimate of $\Delta V/V$ = +5.6% [12].

Phase Diagram of the $Ca_3(PO_4)_2$–$CaNaPO_4$ System

The boundaries of the phase fields in the phase diagram of the $Ca_3(PO_4)_2$–$CaNaPO_4$ system [2] were checked by differential thermal analysis. Crossing phase boundaries while heating is accompanied by an endothermic process. Because the energy of the process is directly proportional to the amount of the substances, to enhance the manifestation of these processes in thermal analysis, the samples of the maximum possible weight for the chosen device (about 130 mg) were taken. The differential thermal analysis data were compared (Fig. 3) with the published phase diagrams of the $Ca_3(PO_4)_2$–$CaNaPO_4$ system; our data turned out to be the closest to Ando and Matsuno's [3].

To refine the compositions of the phase fields in the $Ca_3(PO_4)_2$–$CaNaPO_4$ system, the high-temperature X-ray powder diffraction analysis of the mixtures $(1 - x)Ca_3(PO_4)_2 + xCaNaPO_4$ (x = 0.3, 0.4, 0.6, and 1.0) was performed. The results of this analysis confirmed the differential thermal analysis data and agree with the published data [3] (Fig. 3). Using the results of the

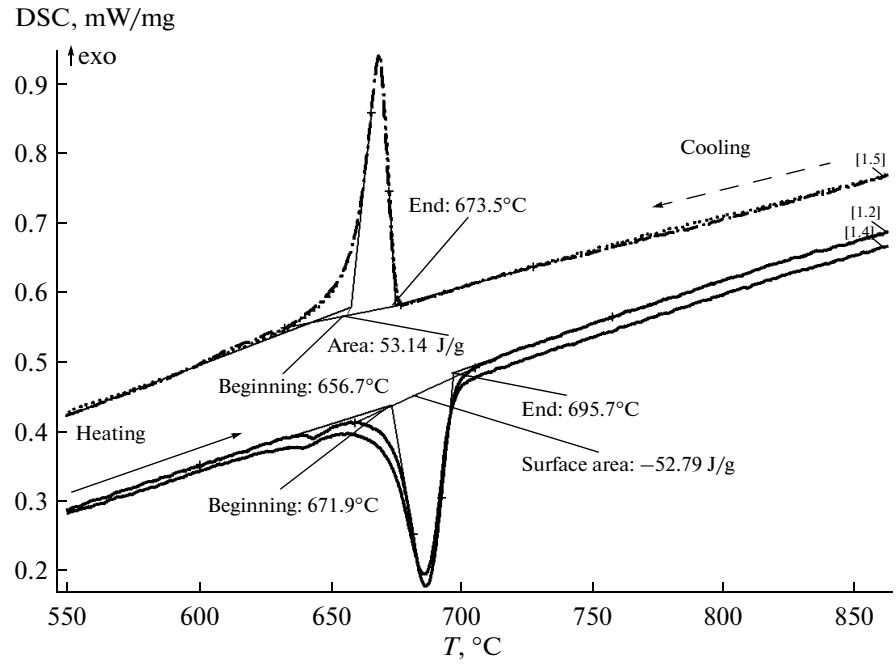

Fig. 2. Differential thermal analysis data on $CaNaPO_4$ (two segments of heating and two segments of cooling).

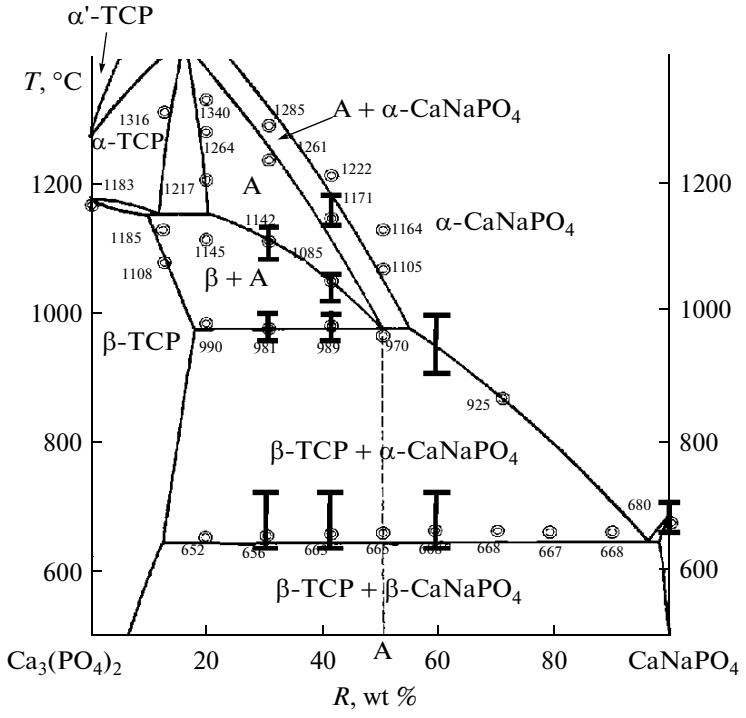

Fig. 3. Phase diagram of the $Ca_3(PO_4)_2$–$CaNaPO_4$ system [2] with the plotted data of differential thermal analysis (circles) and high-temperature X-ray powder diffraction analysis (vertical bars indicating the temperature ranges of observation of phase transformations; the ends of the bars represent the analysis temperatures).

high-temperature X-ray powder diffraction analysis, we also confirmed the temperatures of phase transitions in the studied mixtures that were previously determined by differential thermal analysis.

The boundary of the homogeneity region of the phase β-$Ca_3(PO_4)_2$ can be estimated by measuring the composition dependence of the unit cell parameters of $Ca_{3-x}Na_{2x}(PO_4)_2$ at $x = 0.15 \pm 0.05$. Note that the com-

position $Ca_{10}Na(PO_4)_7$ considered in the literature [13] is within this region, rather than at its boundary.

To refine the region of the existence of the phase A, the mixtures $(1 - x)Ca_3(PO_4)_2 + xCaNaPO_4$ ($x = 0.3$, 0.4) were studied in detail. The high-temperature X-ray powder diffraction analysis gave X-ray diffraction patterns within the temperature range of the existence of the phase A, which were selected using the published data [6, 14] and also the differential thermal analysis data. It can be seen that the X-ray powder diffraction pattern of the phase A mainly coincides with that of α-$CaNaPO_4$ (Fig. 4), except for additional lines, which can be ascribed to the emergence of a superstructure in the process of ordering a solid solution based on α-$CaNaPO_4$. Unlike the known data [6, 15], we recorded the X-ray powder diffraction pattern (Fig. 4) of the pure phase A, which was confirmed by the coincidence of the X-ray patterns for different compositions ($x = 0.3$, 0.4) within the temperature range of the existence of the phase A. Table 1 presents the unit cell parameters of this phase at various temperatures and compositions. The phase A can be described as an ordered solid solution based on α-$CaNaPO_4$ with the 2×3 superstructure, i.e., $a_A = 2a_\alpha$ and $c_A = 3c_\alpha$.

If this phase is considered as relative to nagelschmidtite ($A_7(XO_4)_2(YO_4)_2$ type) owing to the similar values of (Ca + M)/P, then the ordering should be maximal for the composition $Ca_5Na_2(PO_4)_4$, the crystal-chemical formula of which with consideration for the glaserite motif of the partition of the structure into cation {} and cation–anion [] columns can be $\{Ca_4\}[CaNa_2\square(PO_4)_4]$. The superstructure can be due both to the ordering of vacancies (the superstructure along the *a* axis), and to the ordering of calcium and sodium in the cation–anion column (the superstructure along the *c* axis). The general formula of the solid solution A based on nagelschmidtite can thus be written as $\{Ca_4\}[Ca_{1+x/2}Na_{2-x}\square_{1+x/2}(PO_4)_4]$.

Using mixed calcium alkali metal phosphates for producing resorbable bioceramics includes the search for systems the quenching of which from high temperatures should preserve as many as possible of high-temperature polymorphic modifications, in particular, phases with the structure of α-rhenanite or ordered solid solutions on its basis. To determine the optimal compositions with the maximal content of high-temperature phases, we made an experiment in which ceramic samples of binary calcium sodium phosphates of various compositions ($x = 0$–1) were rapidly (at a cooling rate of ~50 deg/min) cooled and the mass ratios in the obtained ceramics were determined. In the middle composition range $x = 0.3$–0.8 (Fig. 5), the rapid cooling from temperatures above the temperature of the invariant equilibrium β-TCP–phase A– α-$CaNaPO_4$ helps producing significant amounts of a phase based on high-temperature α-$CaNaPO_4$ (ordered or unordered, depending on the composition); the best compositions are within the range $x = 0.6$–0.8.

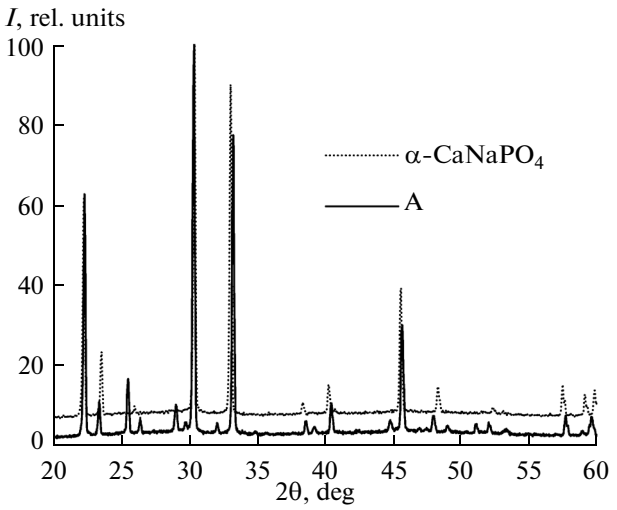

Fig. 4. Comparison of the X-ray powder diffraction patterns of α-$CaNaPO_4$ and the phase A.

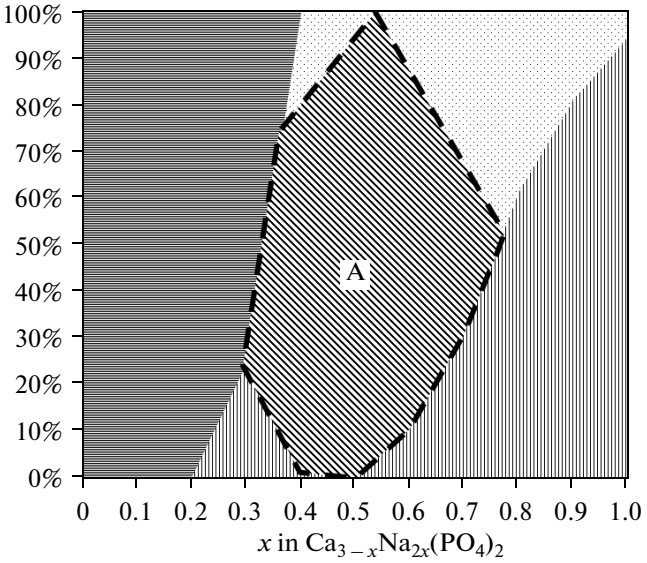

Fig. 5. Contents of the phases of α-rhenanite (points), ordered solid solution based on α-rhenanite (diagonal lines), β-rhenanite (vertical lines), and β-TCP (horizontal lines) in ceramics after quenching from 1200°C.

$CaKPO_4$ Polymorphism

To determine the structural type of the high-temperature phase α-$CaKPO_4$, an experiment similar to that with $CaNaPO_4$ was carried out using Al_2O_3 as an

Table 1. Comparison of the unit cell parameters of the phase A at various temperatures and compositions with the unit cell parameters of the high-temperature phase α-$CaNaPO_4$

$Ca_{3-x}Na_{2x}(PO_4)_2$	*a*, Å	*c*, Å	*V*, Å^3
$x = 0.4$; $T = 1100$°C	10.750(2)	22.598(3)	2261.6(8)
$x = 0.3$; $T = 1200$°C	10.736(2)	22.681(5)	2264.0(1)
$x = 0.4$; $T = 1200$°C	5.383(2)	7.569(2)	190.1(1)

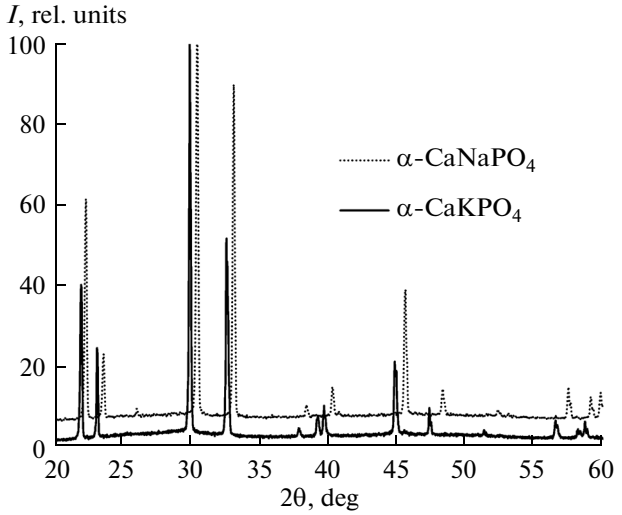

Fig. 6. Comparison of the X-ray powder diffraction patterns of α-$CaNaPO_4$ and α-$CaKPO_4$.

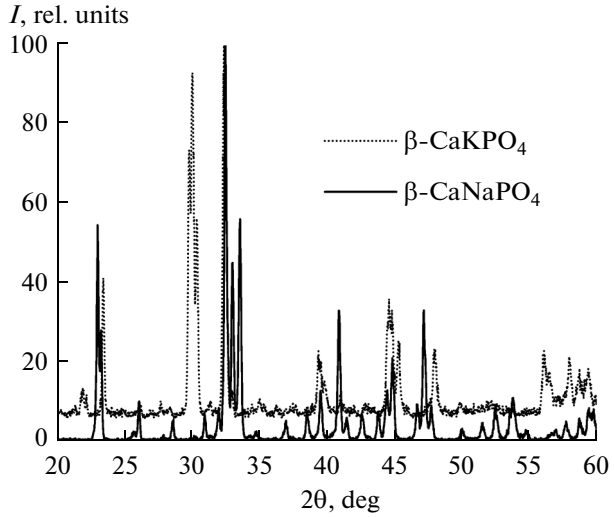

Fig. 7. Comparison of the X-ray powder diffraction patterns of β-$CaKPO_4$ and β-$CaNaPO_4$.

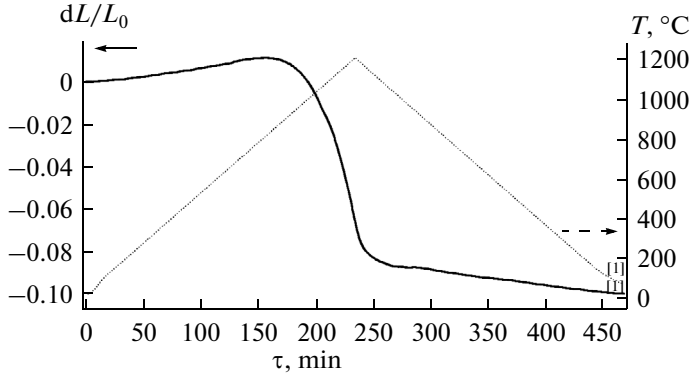

Fig. 8. Dilatometry data on a compact sample of the pure phase $CaKPO_4$.

internal standard. The X-ray powder diffraction pattern (Fig. 6) of α-$CaKPO_4$ fully coincides with α-$CaNaPO_4$, with the difference that the entire X-ray diffraction pattern is shifted toward smaller angles, i.e., that the unit cell parameters are larger (Table 2).

The X-ray powder diffraction pattern of β-$CaKPO_4$ (Fig. 7) shows more reflections than that of β-$CaNaPO_4$, and these reflections are likely to be related to monoclinic distortion of the hexagonal structure of the high-temperature phase α-$CaKPO_4$. One can compare this fact with the transformation α-TCP $\leftrightarrow$ α'-TCP ($P2_1/a \leftrightarrow P\bar{3}m$) [16] and ascertain the structural similarity of the pairs α-TCP, β-$CaKPO_4$ and α'-TCP, α-$CaKPO_4$. However, in comparison with the first-kind fast deformation transition α-TCP $\leftrightarrow$ α'-TCP [11], the transition $\beta \rightarrow \alpha$-$CaKPO_4$ is definitively hindered. According to the differential thermal analysis data, the transition $\beta \rightarrow \alpha$-$CaKPO_4$ occurs within the range 660–860°C (according to the high-temperature X-ray powder diffraction data, ~675 ± 25°C), and the supercooling can exc eed 200°C. The dilatometry showed that the transition $\beta \rightarrow \alpha$-$KCaPO_4$ is accompanied by a negative volume change $\Delta V/V = -2\%$ (Fig. 8).

Thus, in comparison with the transformation $\alpha \rightarrow \beta$-$CaNaPO_4$, the first-kind transition $\alpha \rightarrow \beta$-$KCaPO_4$ is kinetically hindered. This is likely to be caused by the fact that the ionic radius of K is larger than that of Na, which leads to slower displacement of cations in columns and to hindrance to rotation of phosphate tetrahedra. This enables one to obtain a single-phase product comprising only the high-temperature phase α-$CaKPO_4$ by rapid cooling, but, at the same time, makes difficulties in producing a pure phase of the low-temperature modification $CaKPO_4$.

Phase Diagram of the $Ca_3(PO_4)_2$–$CaKPO_4$ System

We failed to find any data on the $Ca_3(PO_4)_2$–$CaKPO_4$ system in the literature, and the results presented below are the first attempt to construct the phase diagram of this system.

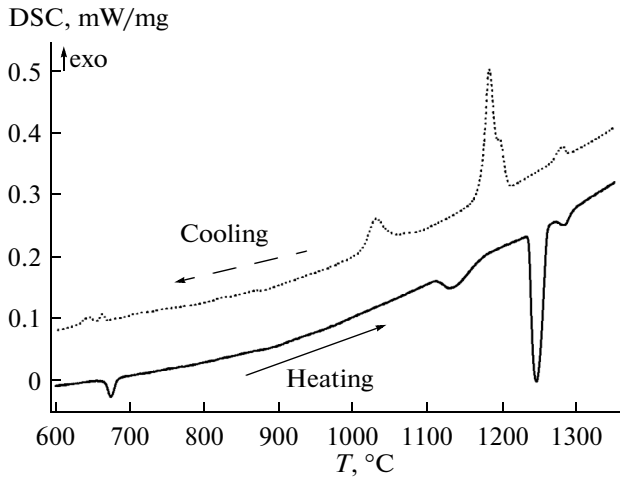

Fig. 9. Differential thermal analysis data for determining phase transformations by the example of $Ca_{3-x}K_{2x}(PO_4)_2$ ($x = 0.3$) (segments of heating and cooling).

The temperatures of the endothermic events detected by the differential thermal analysis (Fig. 9) were plotted in the diagram of the $Ca_3(PO_4)_2$–$CaKPO_4$ system as a function of composition (Fig. 10). To study phase fields of this phase diagram, several high-temperature X-ray powder diffraction experiments were made on the mixtures $(1 - x)Ca_3(PO_4)_2 + xCaKPO_4$ ($x = 0.15$, 0.2, 0.3, 0.33, 0.4, 0.5, 0.6, 0.7, 0.8, and 1.0).

The phase diagram clearly exhibits three isotherms: at 664 ± 5, 1130 ± 5, and 1233 ± 5°C. Considering the phase transitions identified by the differential thermal analysis, we assumed two variants of interpretation of this diagram. One of them is based on the possible existence of a phase of the type A that is observed in the system $Ca_3(PO_4)_2$–$CaNaPO_4$. The other supposes that this phase is absent from this system, and at temperatures above 1130 ± 5°C, there is equilibrium between the phases α-$Ca_3(PO_4)_2$ and α-$CaKPO_4$. The results of a detailed high-temperature X-ray powder diffraction analysis at $x = 0.3$ and 0.6 made us opted for the first variant; however, they also revealed differences from the diagram of the $Ca_3(PO_4)_2$–$CaNaPO_4$ system:

(1) The composition of an intermediate phase and its structure differ from those of the phase A. We called this intermediate phase the phase X;

(2) At temperatures above 1233°C, the phase X transforms to phase B (Fig. 11). A comparison of the unit cell parameters of the phase B and α-$CaKPO_4$ (Table 3) showed that the phase B is a K-containing analogue of the phase A (an ordered solid solution with the 2×3 superstructure) in the $Ca_3(PO_4)_2$–$CaNaPO_4$ system, and the formula of the phase B can be written based on the nagelschmidtite structure as $\{Ca_4\}[Ca_{1+x/2}K_{2-x}\square_{1+x/2}(PO_4)_4]$.

The optimal compositions of ceramic samples (with the maximal content of high-temperature

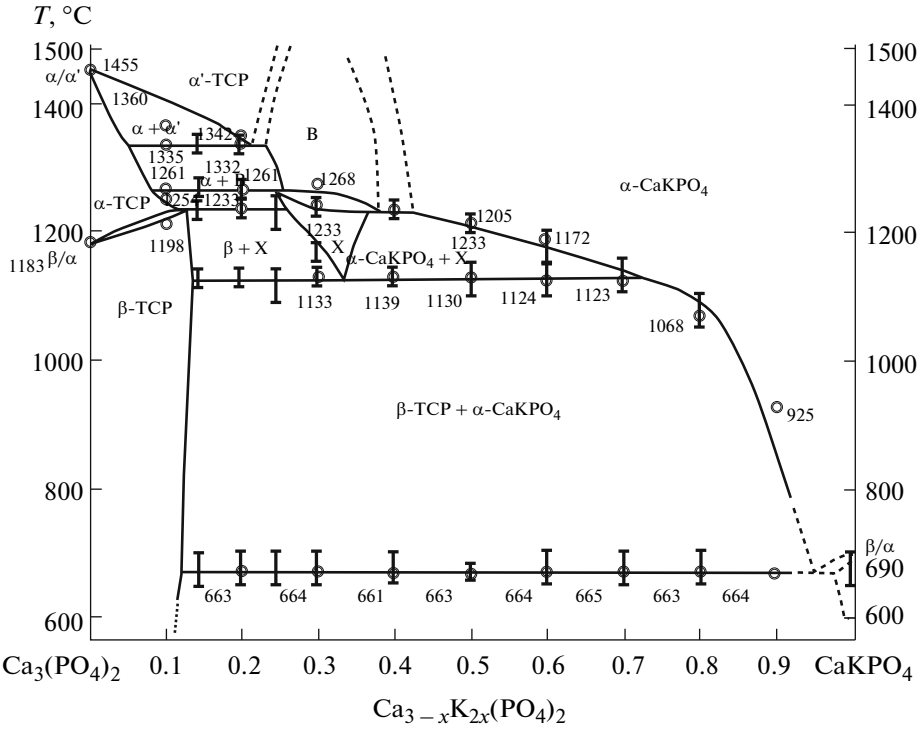

Fig. 10. Phase diagram of the $Ca_3(PO_4)_2$–$CaKPO_4$ system with the plotted data of differential thermal analysis (circles) and high-temperature X-ray powder diffraction analysis (vertical bars indicating the temperature ranges of observation of phase transformations; the ends of the bars represent the analysis temperatures).

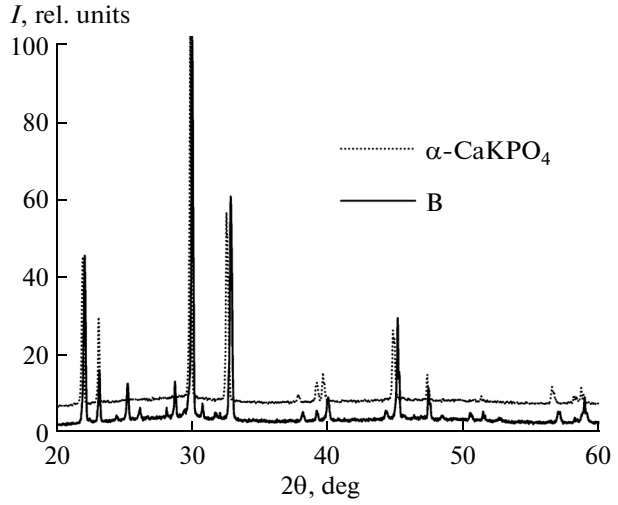

Fig. 11. Comparison of the X-ray powder diffraction patterns of α-$CaKPO_4$ and the phase B.

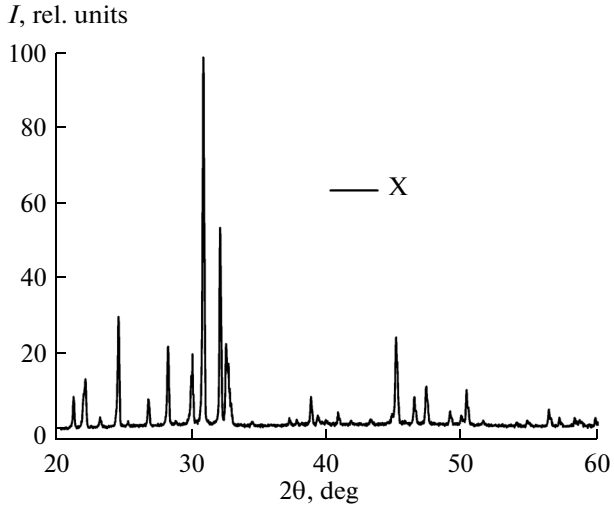

Fig. 12. X-ray powder diffraction pattern of the phase B at 1200°C.

phases) was determined by analogy with the experiment in the $Ca_3(PO_4)_2$–$CaNaPO_4$ system. The content of high-temperature phases in samples turned out to be maximal within the range $x = 0.4$–0.8.

Phase X

All the class of apatites in most cases can be described by two main generalized formulas: $M_{10}(XO_4)_6Y_2$ and $M_{10}(XO_4)_6(\square)_2$ (M = Ca^{2+}, Sr^{2+}, Pb^{2+}, ..., XO_4^{2-}: PO_4^{3-}, VO_4^{3-}, AsO_4^{3-}, ..., Y = F^-, OH^-, Cl^-; and □ is the vacant place of the anion Y).

Apatites identified as $M_{10}(XO_4)_6\square_2$ are stable only when the hexagonal channels are occupied by cations

Table 2. Comparison of the unit cell ($P\bar{3}m1$) parameters of α-$CaKPO_4$ with the unit cell parameters of α-$CaNaPO_4$ at 1200°C

Phase	*a*, Å	*c*, Å	*V*, Å^3
α-$CaKPO_4$	5.615(1)	7.725(2)	210.96(6)
α-$CaNaPO_4$	5.440(5)	7.536(6)	193.16(2)

Table 3. Comparison of the unit cell parameters of the phase B at 1250°C with the unit cell parameters of the high-temperature phase α-$CaKPO_4$

$Ca_{3-x}K_{2x}(PO_4)_2$	*a*, Å	*c*, Å	*V*, Å^3
$x = 0.3$; $T = 1250$°C	10.868(5)	22.94(1)	2709.52(1)
$x = 0.4$; $T = 1250$°C	5.615(1)	7.725(2)	243.55(1)

Tl^+, Pb^{2+}, and Bi^{3+}, which carry lone electron pairs ns^2 located within an empty channel [17]. The possibility of the existence of $Ca_8K_2(PO_4)_6\square_2$ was predicted previously [6]; however, we failed to find any reliable experimental data on the existence of this phase.

The X-ray powder diffraction determined the structural type of the phase X. The obtained X-ray powder diffraction pattern (Fig. 12) is fully indexable (Table 4) within the space group $P6_3/m$ with the unit cell parameters $a = 9.458(1)$ Å and $c = 7.033(5)$ Å. The found unit cell parameters and symmetry type and also the formula of the phase X, $Ca_{6-y}K_xCa_{2+y}K_{2-y}(PO_4)_6\square_2$ (the composition $Ca_{3-x}K_{2x}(PO_4)_2$ at $x = 0.33$ is reduced to integer subscripts), suggest that the phase X has a structure similar to that of apatite, in which the channels constituted by cations at position II (6*h*) are empty. IR spectroscopy detected no vibrations that would be characteristic of the OH group (at ~630 and 3570 cm^{-1}), which is indirectly indicative of the absence of water molecules and, hence, the presence of an empty channel in the apatite structure. We explain the possibility of the existence of such a high-temperature phase (below 1130 ± 5°C, it undergoes eutectoid decomposition into β-TCP and α-$CaKPO_4$) both by the entropy contribution to stabilization by distribution of cations between positions I and II, and by a decrease in the electrostatic repulsion of channel-forming cations because of a decrease in the average charge at positions 6*h* after replacing Ca^{2+} by K^+.

The absence of the phase X in the sodium-containing system implies that the ratio of the ionic radii of the alkali and alkaline-earth metal cations has an effect on the distribution of cations over positions in the apatite structure and, thereby, on the stability of the phase with unoccupied hexagonal channels. We made attempts to obtain similar phases $A_8B_2(PO_4)_{62}$ by combining alkali and alkaline-earth metal cations of different sizes: A = Ca^{2+}, Ba^{2+}; B = K^+, Cs^+. However,

Table 4. X-ray powder diffraction data on $Ca_8K_2(PO_4)\square_2$ at room temperature (assumed space group $P6_3/m$)

d, Å	*I*, %	*hkl*
8.285	39	100
4.761	14	110
4.119	16	200
3.947	13	111
3.538	49	002
3.249	10	102
3.110	35	210
2.848	100	211
2.832	78	112
2.742	92	300
2.677	8	202
2.552	5	301
2.330	1	212
2.280	23	310

the synthesis within the temperature range 1000–1300°C gave no desirable results. Such an experimental fact does not deny the importance of the cation size ratios; rather, it emphasizes the need for searching for a region of stability of the phases $A_8B_2(PO_4)_{62}$ over a wider temperature range.

Thus, the phase equilibria in the quasi-binary sections $Ca_3(PO_4)_2$–$CaMPO_4$ (M = Na, K) are characterized by high-temperature isomorphism of the glaserite-like phases α'-$Ca_3(PO_4)_2$ and α-$CaMPO_4$. Within the composition range close to the pure components, decreasing temperature leads to relatively rapid first-kind deformation phase transitions. In the middle composition range, decreasing temperature is accompanied by cation ordering of a high-temperature solid solution based on α-$MCaPO_4$ to form individual phases.

The main differences of the $Ca_3(PO_4)_2$–$CaKPO_4$ system from the $Ca_3(PO_4)_2$–$CaNaPO_4$ system are the following:

(a) a shift of invariant equilibria toward higher temperatures

(b) deceleration of phase transformations because of lower diffusion mobility of K, which causes, in particular, polymorphism of an intermediate phase of an ordered solid solution based on α-$CaKPO_4$; the low-temperature modification of the composition $Ca_8K_2(PO_4)_6$ has the apatite structure with unoccupied hexagonal channelsæ

(c) the difference of the structure of the low-temperature β-$CaKPO_4$ from that of the sodium-containing analogue, because of which the transformation $\alpha \rightarrow \beta$ is accompanied by an increase in the molar volume.

ACKNOWLEDGMENTS

The study of the diagram of the $Ca_3(PO_4)_2$–$CaKPO_4$ system and the structures of its constituting phases was supported by the Russian Scientific Foundation (project no. 14-19-00752).

This work was performed using equipment purchased within the Program of Development of the Lomonosov Moscow State University.

REFERENCES

1. T. Kanazawa, *Inorganic Phosphate Materials* (Elsevier Science Ltd, Oxford, 1989).
2. J. Ando, Bull. Chem. Soc. Jpn. **31**, 201 (1958).
3. J. Ando and S. Matsuno, Bull. Chem. Soc. Jpn. **41**, 342 (1968).
4. T. Znamierowska, Pol. J. Chem. **55**, 747 (1981).
5. J. Berak and T. Znamierowska, Rocz. Chem. **46**, 1921 (1972).
6. M. A. Bredig, J. Phys. Chem. **46**, 747 (1942).
7. F. H. Chung, J. Appl. Crystallogr. **7**, 526 (1974).
8. T. Ozawa, Bull. Chem. Soc. Jpn. **38**, 1881 (1965).
9. J. H. Flynn and L. A. Wall, J. Polym. Sci., Part B: Polym. Lett. **4**, 323 (1966).
10. S. Vyazovkin, J. Therm. Anal. Cal. **83**, 45 (2006).
11. P. V. Evdokimov, V. I. Putlyaev, D. A. Merzlov, et al., Nanosist.: Fiz. Khim. Mat. **4**, 48 (2013).
12. V. I. Putlayev, P. V. Evdokimov, A. V. Garshev, et al., Rus. Phys. J. **56**, 1183 (2014).
13. V. A. Morozov, A. A. Belik, R. N. Kotov, et al., Crystallogr. Rep. **45**, 13 (2000).
14. J. M. Millet, A. Sebaoun, and G. Thomas, J. Therm. Anal. **29**, 445 (1984).
15. G. Celotti and E. Land, J. Eur. Ceram. Soc. **23**, 851 (2003).
16. M. Yashima and A. Sakai, Chem. Phys. Lett. **372**, 779 (2003).
17. M. Azrour, M. Azdouz, B. Manoun, et al., J. Phys. Chem. Solids **72**, 1199 (2011).

Translated by V. Glyanchenko